N85-31635

MEASUREMENT OF ELECTRICAL PARAMETERS AND CURRENT COMPONENTS IN THE BULK OF SILICON SOLAR CELLS

Arnost Neugroschel
Department of Electrical Engineering
University of Florida
Gainesville, FL 32611

ABSTRACT

A review and illustration of electrical measurements for determination of the bulk parameters in silicon solar cells is given. The presentation concentrates on transient and small-signal admittance measurements. These measurements yield accurate and reliable values of the base lifetime and the surface recombination velocity at the back contract without inaccuracies that normally results from electrons and holes in the p/n junction space-charge region. This then allows the determination of the recombination current in each region of the cell. As an example, current components in the emitter, low-doped base, high-doped base and junction space-charge region of the back-surface field cell are obtained. Such analysis is essential in determining the relative importance of the base and the emitter and, thus, the region that limits the cell efficiency.

I. INTRODUCTION

The efficiency of state-of-the-art solar cells is determined primarily by the minority-carrier diffusion length in the base of the cell and for some cells also by the surface recombination velocity at the back contact. It is, thus, very important to have measurement methods for fast and reliable determination of these two parameters.

Various methods are available at the present, some of which were reviewed by others [1]. In this presentation we concentrate on two methods only: (1) the short-circuit-current decay method [2], and (2) the small-signal-admittance methods [3-5]. It will be demonstrated that these two approaches yield reliable results directly from the data without any adjustable parameters which are usually taken from the literature when using some other techniques. The methods also allow the determination of the relative importance of the base and the emitter regions of the cells.

II. SHORT-CIRCUIT CURRENT DECAY (SCCD)

This is a relatively new method described in detail in [2]. We will describe it here only briefly. A solar cell is forward-biased with voltage V causing forward current I_f. At time t=0, the cell is short-circuited through a fast and very low resistance MOS transistor, by applying a voltage pulse to the

gate, see Fig. 1(a). The current transient measured across a small resistor R is displayed on an oscilloscope. The current transient can be expressed as an infinite series of exponential decays

$$i(t) = \sum_{i=1}^{\infty} i_i(0)\, e^{-t/\tau_{di}} \equiv i(0)e^{-t/\tau_d} + \sum_{i=2}^{\infty} i_i(0)\, e^{-t/\tau_{di}} \qquad (1)$$

where τ_{di} is the decay time constant of the i-th mode and $i_i(0)$ is the corresponding initial value at t=0. As shown in [2] the first mode is dominant and the higher decay modes can be neglected. The value of the first-mode τ_d is obtained simply from the $\log_e i(t)$ vs t plot, and the corresponding i(0) is obtained by extrapolating the straight portion of the plot to t=0. This extrapolation is necessary partly because the delay time constant of the measurement circuit prevents accurate measurement immediately after the closing of the switch. The resulting plot is schematically illustrated in Fig. 1(b). Figure 1(c) shows the measured current decay for a $n^+/p/p^+$ back-surface-field (BSF) solar cell with $\tau_d = 6.4$ μsec yielding $L_n = 180$ μm, $S_{eff} = 1.3 \times 10^3$ cm/sec.

The two measured quantities, i(0) and τ_d, are both functions of the minority-carrier base lifetime τ and the effective surface recombination velocity S_{eff} at the back contact. Simultaneous solution of these two dependencies (see Appendix A) yields the desired parameters: τ and S_{eff}.

The discharging of the excess electrons and holes in the junction space-charge-region (SCR) occurs within a time of the order of $\sim 10^{-11}$ sec. The discharging of the excess carriers in the emitter occurs within a time about equal to the emitter lifetime or emitter transit time, both of which are much smaller than the first-mode τ_d. As a result, the SCR and the emitter do not affect the transient observed on a time scale about equal to τ_d.

This fact is one of the main advantages of this method of measurement of the base properties in comparison with more conventional transient methods, such as the open-circuit voltage decay (OCVD) and the reverse-step recovery (RSR). As discussed in detail in [2], both the OCVD and the RSR methods suffer from distortions caused by the recombination within the SCR and the emitter that persist throughout the entire decay.

The sensitivity of the SCCD method to the bulk lifetime and to the surface recombination velocity is illustrated in Figs. 2(a) and 2(b). These figures show that for thin cells with W << L, the SCCD method is very sensitive to S_{eff} but rather insensitive to τ. For cells with W >> L, the method is very sensitive to τ but insensitive to S_{eff}. This behaviour can be explained by realizing that if W << L, then most of the minority carriers recombine at the back surface. However, if W >> L, then most of the recombination occurs in the bulk.

In the two limiting cases above, the SCCD technique will yield only one of the desired parameters, either L or S. In order to determine the other parameter for these two cases, the SCCD measurement has to be supplemented by

some other external charcteristic of the cell dependent on both S and L. For example, one can use the dark saturation current I_D or the open-circuit voltage V_{oc} for this purpose. Both I_D and V_{oc}, however, may be affected by the emitter region and the combination of SCCD - I_D or SCCD - V_{oc} may give misleading results for the base parameters.

In the next section we explore small signal admittance techniques that are sensitive primarily to the base properties. The combination of the SCCD and the admittance techniques gives the base parameters (S, L) for any cell regardless of the W/L ratio.

III. SMALL-SIGNAL ADMITTANCE MEASUREMENTS [3-5]

Small-signal admittance measurements can be used to analyze a variety of semiconductor devices. We discuss here specifically the applications for analyzing the solar cells, namely measurement of the base L and S_{eff} and the separation of the emitter and the base current components. The small-signal measurements can be performed either at low-frequencies ($\omega\tau << 1$) or high frequencies ($\omega\tau >> 1$). The choice of a particular frequency range will depend on the W/L ratio.

A. Low-frequency method (LF) [3,4]

Consider a $n^+/p/p^+$ BSF solar cell shown in Fig. 3(a). For a low-frequency signal with $\omega\tau_n << 1$, where τ_n is the minority-carrier electron lifetime in the p-type base, we derive the expressions for the small-signal quasi-neutral base capacitance C^{LF}_{QNB} and conductance G^{LF}_{QNB}, respectively (see equations (B1) and (B2) in Appendix B). Equations (B1) and (B2) contain four unknowns: C^{LF}_{QNB}, G^{LF}_{QNB}, L_n, and S_{eff}. The parameters C^{LF}_{QNB} and G^{LF}_{QNB} are measured and the combination of (B1) and (B2) yields L_n and S_{eff}.

It is worthwhile to discuss in more detail a few special cases:

A.1 Long diode: W > L

For this case, (B1) and (B2) yield a simple expression for C^{LF}_{QNB} and τ_n

$$C^{LF}_{QNB} = \frac{q}{kT}\frac{Aqn_i^2 L_n}{2N_{AA}}\left[\exp\left(\frac{qV}{kT}\right) - 1\right] \qquad (2)$$

and

$$\tau_n = \frac{2C^{LF}_{QNB}}{G^{LF}_{QNB}} \quad . \qquad (3)$$

The base diffusion length is obtained either from (2) or from (3). The details concerning the deduction of C^{LF}_{QNB} and G^{LF}_{QNB} from the data are discussed in [3]. As an illustrative example, we show in Fig. 4 the measured $C^{LF}_{QNB}(V)$ and

$G^{LF}_{QNB}(V)$ plots for the p^+/n device with $N_{DD} = 1.25 \times 10^{15} cm^{-3}$. The analysis using (3) or (3) gives $L_p = 80$ μm.

A.2 BSF solar cell: $W_p \lesssim L_n$, $W_p D_n/L_n^2 < S_{eff} < (D_n\ W_p)$

In this case, (B1) and (B2) are solved to yield L_n and S_{eff}. Figure 5 shows the measured C(V) and G(V) dependencies for a $p^+/n/n^+$ BSF solar cell from which we derive $L_p = 500$ μm and $S_{eff} = 80$ cm/sec.

The method fails, however, for $S_{eff} << D_n\ W/L_n^2$; in this case $G^{LF}_{QNB} = KW_p/\tau_n$ yields τ_n, but S_{eff} cannot be found. Another limitation exists for high values of $S_{eff} >> D_n/W_p$; in this case both (B1) and (B2) are independent of L_n and S_{eff}.

The above difficulties with the LF method can be largely eliminated by the high-frequency approach.

B. High-frequency method (HF) [5]

We treat the high frequency method for two special cases.

B.1 $\omega\tau_n > 10$ and $0.1 \lesssim W_p/L_n \lesssim 1$

The small-signal admittance then is

$$Y^{HF}_{QNB} = \frac{KD_n}{L_n}\left[\left(\frac{\omega\tau_n}{2}\right)^{1/2} + j\omega\left(\frac{\tau_n}{2\omega}\right)^{1/2}\right] = G^{HF}_{QHB} + j\omega\, C^{HF}_{QNB} \quad . \tag{4}$$

The important conclusion from (4) is that the $\omega^{1/2}$ dependence gives the range of $0.1 \lesssim W_p/L_n \lesssim 1$ regardless of the value of S_{eff}. To obtain the desirable parameters, we measure G^{HF}_{QNB} vs ω for $\omega\tau \gtrsim 10$ and extrapolate to lower frequencies to obtain an intercept ω_I with G^{LF}_{QNB} given by (B2). This gives

$$L_n^2 = \left(\frac{2\ W_p^2\ D_n}{\omega_I}\right)^{1/2} \left(\frac{D_n}{W_p}\right) \frac{1 + (S_{eff} L_n^2/D_n W_p)}{(D_n/W_p) + S_{eff}} \tag{5}$$

Equation (5) cannot be be solved for L_n and S_{eff} except for the following cases:

a) $S_{eff} < D_n W_p/L_n^2 < D_n/W_p$

$$L_n = (2W_p^2 2D_n/\omega_I)^{1/4} \tag{6}$$

b) $D_n W/L_n^2 < S_{eff} < D_n/W_p$

$$S_{eff} = (\omega_I D_n/2)^{1/2} \quad . \tag{7}$$

The method is illustrated in Fig. 6 for the $p^+/n/n^+$ solar cell of Fig. 5. G^{HF}_{QN} follows the $\omega^{1/2}$ dependence for $f \gtrsim 10^4$ Hz with the intercept at $\omega_I =$

$(2\pi)10^3$ 1/sec. Using (5) and combining with $S_{eff} \approx 80$ cm/sec obtained by the LF method, we have $L_p \approx 503$ μm, which is in excellent agreement with $L_p \approx 500$ μm using the LF method alone.

Even though the general solution (5) cannot give L and S_{eff} exactly, and only one of the parameters is obtained either from (6) or from (7), the method is very useful because: (i) the G_{QN}^{HF} vs $\omega^{1/2}$ dependence shows that L > W; (ii) the G_{QN}^{HF} vs $\omega^{1/2}$ dependence indicates that the emitter contribution to the conductance (and dark current) is negligible (this point is discussed further below); (iii) the SSCD for L > W yields an accurate value of S_{eff} only and using this value in (5) we obtain an accurate value for L. The combination of these two methods gives L and S_{eff} for practically any cell.

The sensitivity of the HF method to the emitter component G_{QNE}^{HF} of the total measured quasi-neutral conductance $G_{QN}^{HF} = G_{QNB}^{HF} + G_{QNE}^{HF}$ is explored in Fig. 7. The time constant τ_E of G_{QNE}^{HF} is given by either the Auger lifetime τ_A in the heavily doped emitter, or by the combination of τ_A and the transit time [6]. The emitter time constant is much shorter than the base lifetime, thus G_{QNE}^{HF} is frequency independent up to $f \approx 1/\tau_E \gg 1/\tau_B$. Figure 7 shows $G_{QN}^{HF} = G_{QNB}^{HF} + G_{QNE}^{HF}$ for an arbitrary choice of $G_{QNE}^{HF}/G_{QNB}^{HF}$. The region far away from the knee can be fitted to a straight line with $G \propto \omega^{1/m}$, where m > 2. Notice, however, that ω_I for $G_{QNE}^{HF} > 0$ is close to the intercept value ω_I for $G_{QNE}^{HF} = 0$. Furthermore, since $L \propto \omega_I^{-1/4}$, a small error in ω_I gives only a negligible error in L. For example, for $G_{QNE}^{HF} = G_{QNB}^{HF}$, $\omega_I \approx 1.5\ \omega_I$ ($G_{QNE}^{HF} = 0$), this gives an error in L of only about 10%.

B.2 $\omega\tau_n > 10$, $W_p/L_n \leq 0.1$

The condition $W_p/L_n \leq 0.1$ may apply for the thin cells (50 - 100 μm) with a very long lifetime. For this case we have

$$G_{QN}^{HF} \approx KD_n \frac{(\omega^2 W_p^3/3) + S_{eff}(D_n + S_{eff}W_p)}{(D_n + S_{eff}W_p)^2} \quad . \tag{8}$$

For BSF cells, $S_{eff} < D_n/W_p$ and (8) yields

$$G_{QN}^{HF} \approx K[\omega^2(W^3/3D_n) + S_{eff}] \quad . \tag{9}$$

Figure 8 shows the G_{QN}^{HF} vs ω dependence for a 8 μm thick epitaxial n-type layer with doping density $N_{DD} = 5 \times 10^{15}$ cm^{-3}. The ω^2 dependence for f > 1.5 MHz immediately gives $L_p > 10W > 80$ μm and also $S_{eff} \ll \omega^2W^3/3D_n \ll 1.2 \times 10^3$ cm/sec. More accurate analysis of the knee region below the ω^2 dependence gives $S_{eff} \approx 120$ cm/sec and using this value in (B1) gives more accurate $L_p \approx 90$ μm.

Note, that the HF method for L > 10 W gives only the lower limit of L and the upper limit of S_{eff}. A combination of this technique with either the LF method or the SCCD can give more accurate results.

B.3 $\omega\tau_n \sim 10$, $W_p/L_n \sim 0.1$

For the previous two special cases we have obtained $G_{QNB}^{HF} \propto \omega^{1/2}$ for $W_p/L_n \lesssim 0.1$ and $G_{QNB}^{HF} \propto \omega^2$ for $W_p/L_n \lesssim 0.1$. Obviously, there has to be an intermediate range for $W_p/L_n \sim 0.1$ where $G_{QNB}^{HF} \propto \omega^m$ ($< m \lesssim 2$). One possible approach here is to obtain S_{eff} from the SCCD method and then fit the theoretical $G_{QN}^{HF}(S_{eff}, L_n)$ with the experiment. A very reasonable approximation of τ_n can be made, however, by realizing that the G_{QN} vs ω dependence begins to increase from its low-frequency value for $\omega = \omega_I \approx 10/\tau_n$ [5]. Thus, $\tau_n \approx 10/\omega_I$, where ω_I can be approximated as the intercept of the G_{QN}^{LF} line with the extrapolated $G_{QN}^{HF} \propto \omega^m$ dependence.

IV. REGIONAL ANALYSIS OF SOLAR CELLS

It is important to analyze the contributions of each region of the cell to the total dark current (or V_{oc}). Such an analysis is demonstrated here for a $n^+/p/p^+$ BSF solar cell shown in Fig. 3(b). The analysis is based on the determination of the base parameters τ_n and S_{eff} by one of the methods discussed in Section II and III. This is sufficient to calculate the profile of the minority electrons in the base. The recombination losses in the base are given by (B2) and the recombination losses in the p^+-BSF portion of the base are

$$I_n(W_p) = I_B^+ = AqS_{eff}N(W_p) \quad . \tag{10}$$

The SCR recombination current I_{SCR} can be determined graphically [7] and the emitter contribution I_E is obtained by realizing that the total dark current is

$$I_D = I_E + I_{SCR} + I_B + I_B^+ \quad . \tag{11}$$

For example,such analysis of the $p^+/n/n^+$ BSF cell of Fig. 5 gave [4]: $L_p \approx 500$ μm, $S_{eff} \approx 80$ cm/sec, $I_B \approx 0.8\ I_D$, $I_{SCR} \approx 0.2\ I_D$, $I_E \ll I_D$, $I_B^+ \ll I_D$.

V. SUMMARY

Table I gives a summary of results for a number of different cells. A comparison of results obtained by different methods, shown for some cells, demonstrates very good agreement. Notice, in particular, the last cell in Table I, which is a thin cell (W_{base} - 92 μm) with $L_n > W_B$. For this cell, the SCCD method gives $S_{eff} \approx 180$ cm/sec, but the meth[illegible] is insensitive to L_n (see Fig. 2(a)). We have to combine the SCCD method with the high-frequency small-signal admittance method and then use (5) with S_{eff} obtained from the SCCD method to determine L_n.

The main conclusion of this study is that the SCCD method and the small-signal admittance methods yield a rapid and reliable determination of the base

parameters. They also allow the determintion of the relative importance of the base and the emitter regions with regard to cell efficiency. Identification of the region limiting the efficiency is a key to an informed cell design.

Acknowledgement: This work was supported in part by NSF Grant No. ECS-8203091.

APPENDIX A

To obtain the base diffusion length L and effective surface recombination velocity S_{eff} at the back contact we have to solve the following two equations for the first-mode decay [2]:

$$1 + (D_p K_1/L_p S_{eff})\cot(W_{QNB}K_1/L_p) = 0 \qquad (A1)$$

$$i(0) = -\frac{qD_p P(0,0^-)K_1}{S_1 L_p}\,\frac{\cot(K_1 W_{QNB}/L_p) - (D_p K_1/L_p S_{eff})}{(\tau_p/2K_1^2) + (W_{QNB}/2S_{eff})[\mathrm{cosec}^2(K_1 W_{QNB}/L_p)]} \qquad (A2)$$

Here $K_1 = (-1 - S_1\tau_p)^{1/2}$, $S_1 = -1/\tau_{D1}$, W_{QNB} is the width of the quasi-neutral base, and $P(0, 0^-) = (n_i^2/N_{DD})[\exp(qV/kT) - 1]$ where V is the steady forward voltage applied for $t < 0$.

APPENDIX B

The small-signal quasi-neutral base capacitance and conductance are given by [4]:

$$C_{QNB}^{LF} = \frac{KD_n}{2L_n}\left[\frac{\frac{W_p D_n}{L_n} - \frac{L_n W_p^2 S_{eff}}{D_n} - S_{eff}L_n}{(\sinh^2\frac{W_p}{L_n})(\frac{D_n}{L_n}\coth\frac{W_p}{L_n} + S_{eff})^2} + \right.$$

$$\left. + \tau_n \frac{\frac{D_n}{L_n} + S_{eff}\coth\frac{W_p}{L_n}}{\frac{D_n}{L_n}\coth\frac{W_p}{L_n} + S_{eff}}\right] \qquad (B1)$$

$$G_{QNB}^{LF} = \frac{KD_n}{L_n}\,\frac{\frac{D_n}{L_n} + S_{eff}\coth\frac{W_p}{L_n}}{\frac{D_n}{L_n}\coth\frac{W_p}{L_n} + S_{eff}} \qquad (B2)$$

where $K = Aq(q/kT)(n_i^2/N_{AA})\exp[(qV/kT) - 1]$.

Table I: Summary of results for some typical solar cells. The values for L_{base} and S_{eff} were obtained using the SSCD method, unless marked otherwise

CELL	ρ_{base} (Ωcm)	W_{base} (μm)	L_{base} (μm)	S_{eff} (cm/sec)
$n^+/p/p^+$	10	227	454	105
BSF			450*	
$n^+/p/p^+$	10	103	250	2.9×10^3
BSF				
$n^+/p/p^+$	10	360	512	2×10^5
$n^+/p/p^+$	0.15	295	100	---
$p^+/n/n^+$	10	320	303* 500†	80†
BSF				
$n^+/p/p^+$	10	92	~600*	~180
BSF				

* obtained from G_{QN}^{HF}

† obtained from G_{QN}^{LF}

REFERENCES

1. J. H. Reynolds and A. Meulenberg, Jr., J. Appl. Phys., 45, 2582 (1974); A. Azim Khan, J. A. Woolam, and A. M. Hermann, Appl. Phys. Commun., 2, 17(1982).

2. T. W. Jung, F. A. Lindholm, and A. Neugroschel, IEEE Trans. Electron Devices, ED-31, 588(1984).

3. A. Neugroschel, P. J. Chen, S. C. Pao, and F. A. Lindholm, IEEE Trans. Electron Devices, ED-25, 485(1978).

4. A. Neugroschel, IEEE Trans. Electron Devices, ED-28, 108(1981).

5. F. N. Gonzalez, A. Neugroschel, IEEE Trans. Electron Devices, ED-31, 413(1984).

6. M. A. Shibib, F. A. Lindholm, and F. Therez, IEEE Trans. Electron Devices, ED-26, 959(1979).

7. A. Neugroschel, F. A. Lindholm, and C. T. Sah, IEEE Trans. Electron Devices, ED-24, 662(1977).

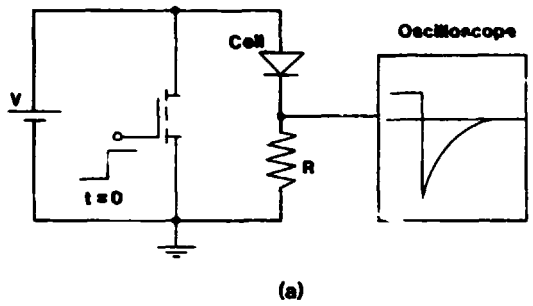

(a)

Fig. 1. (a) Electronic circuit used in the SCCD method. The switching time of a power MOST is less than 100 nsec.

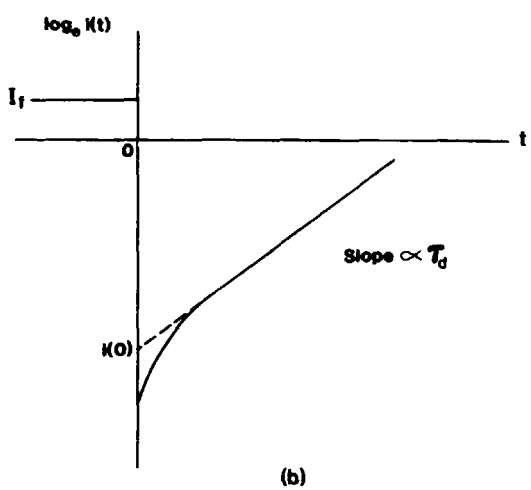

(b)

(b) Schematic illustration of the current decay displayed on a log scale.

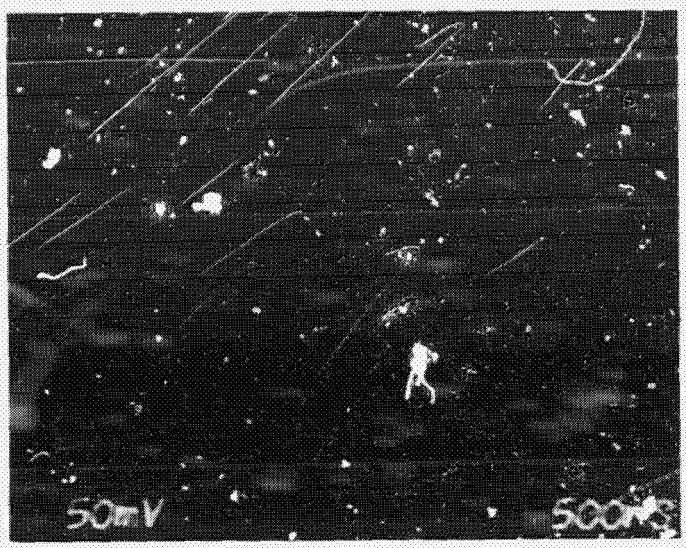

(c) Experimental current decay for a $n^+/p/p^+$ BSF solar cell ($\rho_{base} \simeq 0.3$ Ωcm, $W_{base} \simeq 367$ μm, $\tau_d \simeq 6.4$ μsec, $L_n \simeq 180$ μm, $S_{eff} \simeq 1.. \times 10^3$ cm/sec). The vertical scale is 100 mA/division.

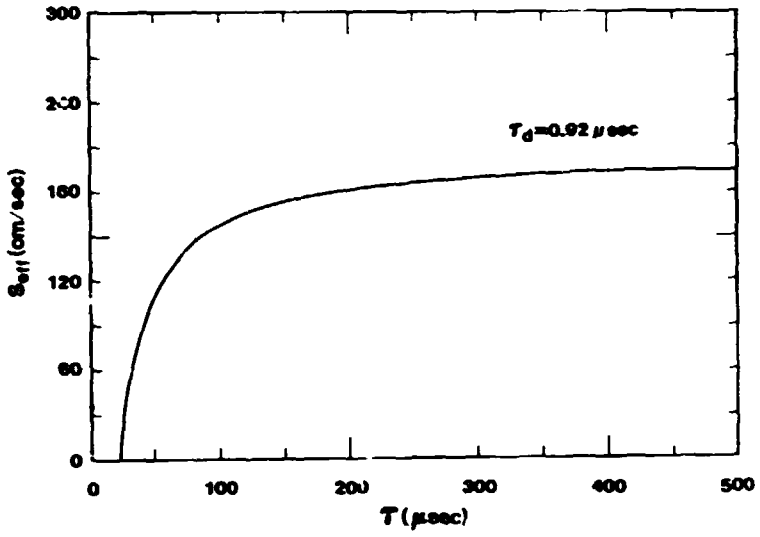

(a)

Fig. 2. (a) Plot of S_{eff} vs τ for a thin $n^+/p/p^+$ BSF solar cell (ρ_{base} = 10 Ωcm, W_{base} = 32 μm).

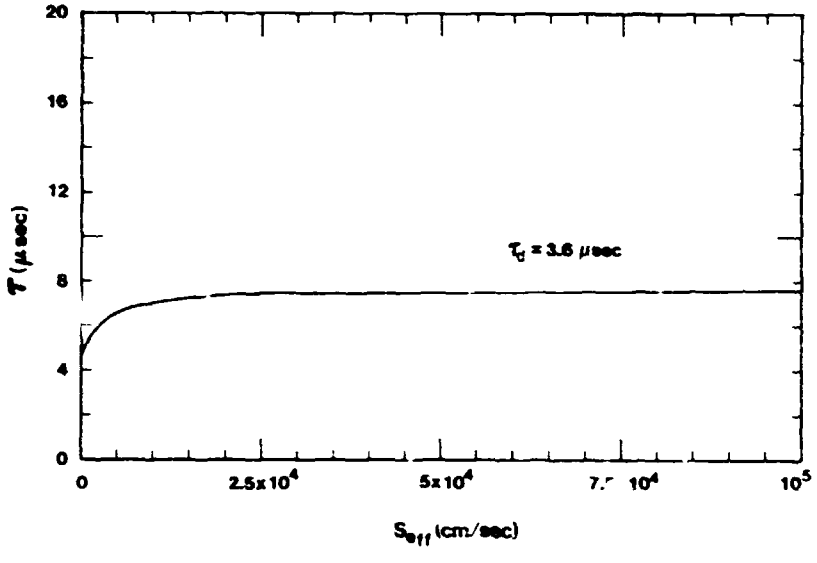

(b)

(b) Plot of τ vs S_{eff} for a thick $n^+/p/p^+$ BSF solar cell (ρ_{base} = 0.15 Ωcm, W_{base} = 295 μm).

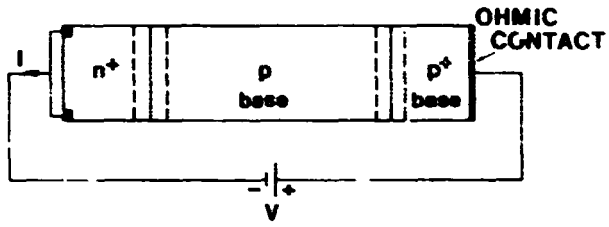

(a)

$$I = I_E + I_{SCR} + \frac{q}{\tau_n}\int_0^{W_p} N(x)\,dx + I_{B^*}$$

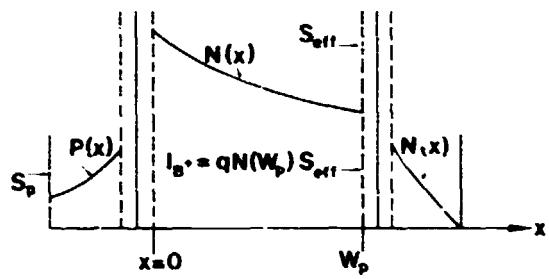

(b)

Fig. 3 (a) Schematic diagram of an $n^+/p/p^+$ BSF solar cell.
(b) Qualitative sketches of minority-carrier distributions in the dark.

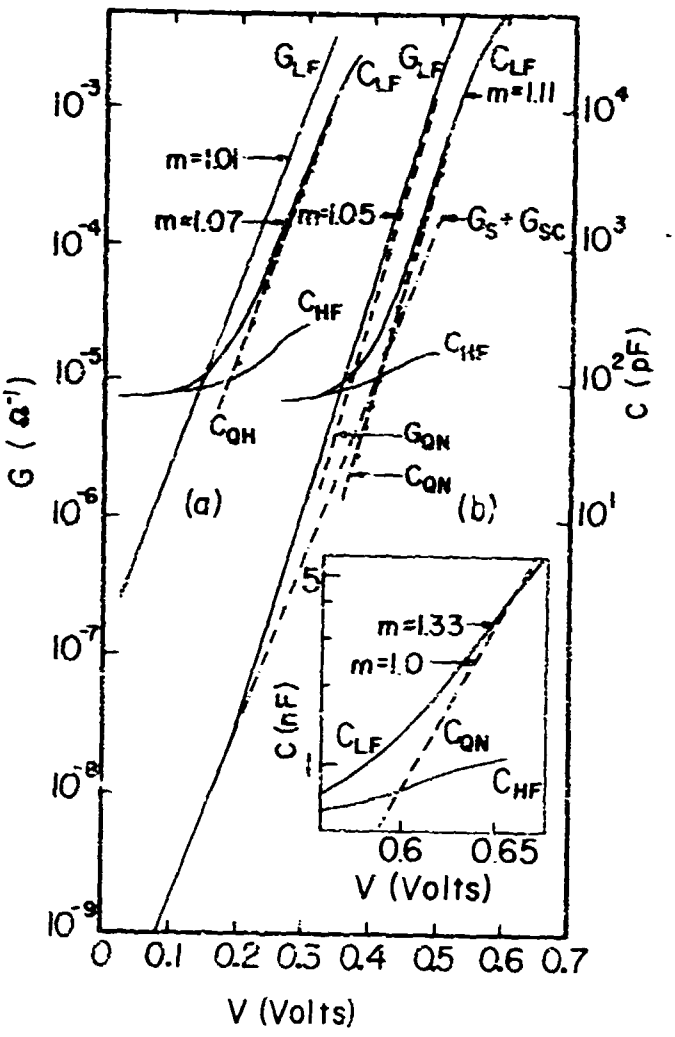

Fig. 4 Measured conductance and capacitance vs forward-bias V for a long p^+/n diode with $N_{DD} = 1.25 \times 10^{15}$ cm^{-3} and $W_{base} = 250$ μm (from Ref. [3]).

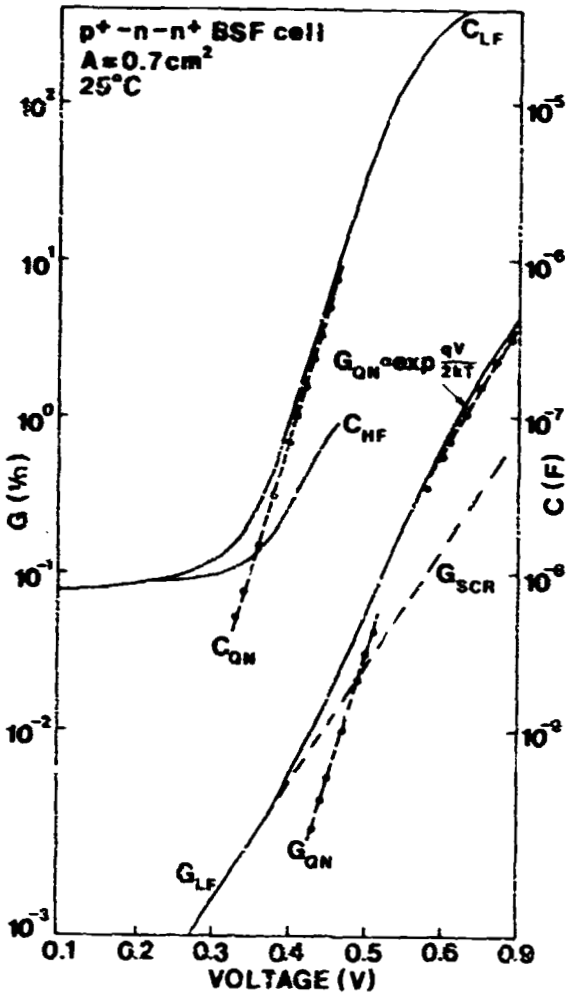

Fig. 5 Measured capacitance and conductance vs forward bias for a $p^+/n/n^+$ BSF solar cell (from Ref. [4]). Here, $N_{DD} = 6 \times 10^{14}$ cm^{-3}, $W_{base} = 320$ μm.

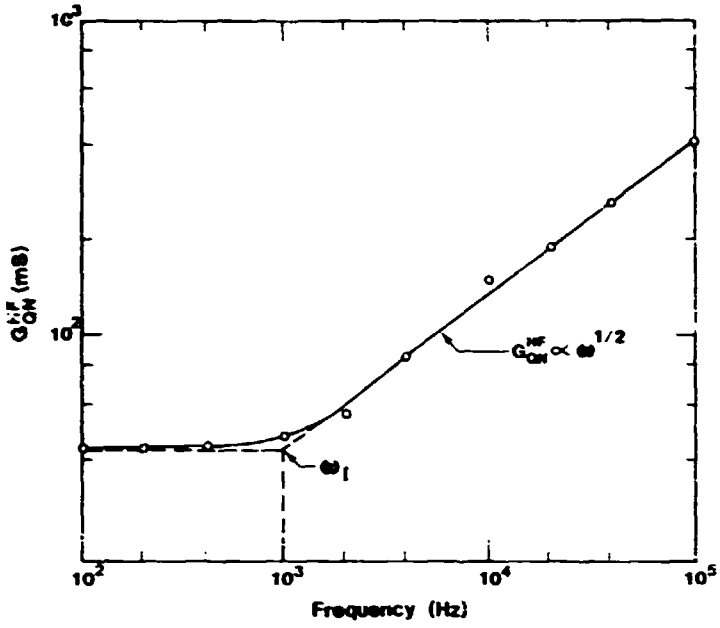

Fig. 6. Measured high frequency conductance G_{ON}^{HF} vs freqency for the $p^+/n/n^+$ solar cell of Fig. 5. The conductance was measured at forward bias V = 0.5 V and shows $\omega^{1/2}$ dependence.

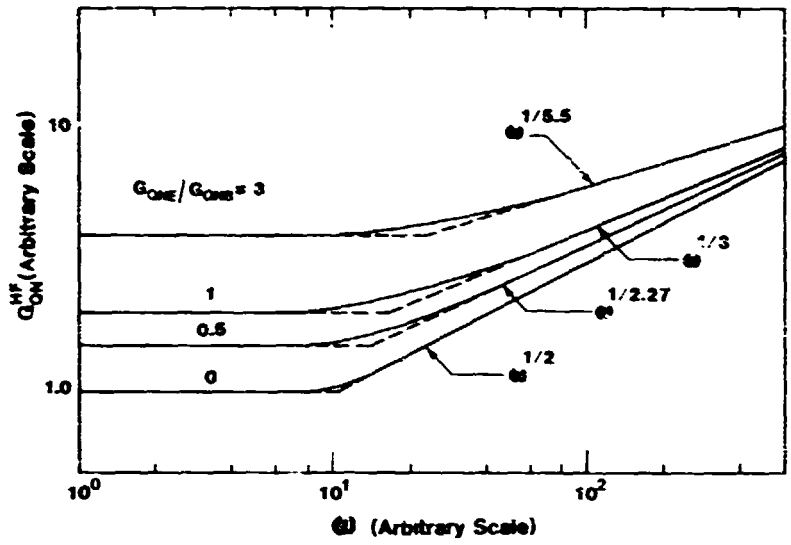

Fig. 7. Plot of a $G^{HF}_{QN} = G^{HF}_{QNB} + G^{HF}_{QNE}$ for different ratios of $G^{HF}_{QNE}/G^{HF}_{QNB}$ = 0, 0.5, 1, 3.

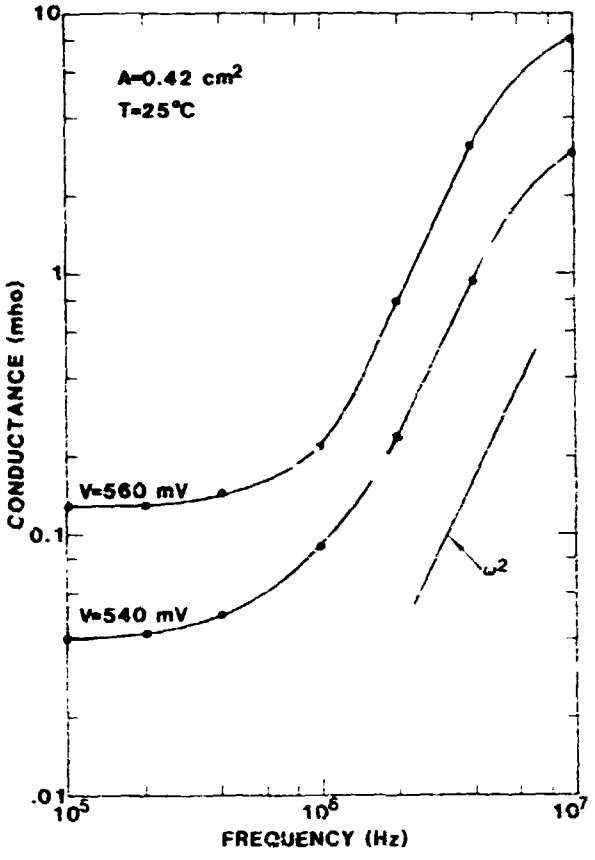

Fig. 8 Frequency dependence of high-frequency conductance for a thin (8 μm) n-type epitaxial layer (from Ref. [5]). The conductance follows ω^2 dependence.

VON ROOS: You made one comment I would to talk about, and that was the diffusion length -- if it is much larger then the width of the cell, it cannot be measured by any other means. Now, that is not quite correct. There is another means to do that, and that is with the EBIC or amplitude-modulated electron beam; measuring the phase shift will indeed give you the lifetime, and therefore the diffusion length -- also in the case where the ratio of width over diffusion length is very small.